THE JOURNAL OF PHYSICAL CHEMISTRY B

Article

Cite This: J. Phys. Chem. B 2019, 123, 5769−5781

pubs.acs.org/JPCB

Chiral Inversion of Amino Acids in Antiparallel β-Sheets at Interfaces Probed by Vibrational Sum Frequency Generation Spectroscopy

Published as part of The Journal of Physical Chemistry virtual special issue "Hai-Lung Dai Festschrift".

Ethan A. Perets,[†,§] Pablo E. Videla,[†,‡,§] Elsa C. Y. Yan,[*,†] and Victor S. Batista[*,†,‡]

[†]Department of Chemistry, Yale University, 225 Prospect Street, New Haven, Connecticut 06520, United States

[‡]Energy Sciences Institute, Yale University, 810 West Campus Drive, West Haven, Connecticut 06516, United States

Supporting Information

ABSTRACT: A parallel study of protein variants with all (L-), all (D-), or mixed (L-)/(D-) amino acids can be used to assess how backbone architecture versus side chain identity determines protein structure. Here, we investigate the secondary structure and side chain orientation dynamics of the antiparallel β-sheet peptide $LK_7\beta$ (Ac-Leu-Lys-Leu-Lys-Leu-Lys-Leu-NH_2) composed of all (L-), all (D-), or alternating (L-Leu)/(D-Lys) amino acids. Using interface-selective vibrational sum frequency generation spectroscopy (VSFG), we observe that the alternating (L-)/(D-) peptide lacks a resonant C−H stretching mode compared to the (L-) and (D-) variants and does not form antiparallel β-sheets. We rationalize our observations on the basis of density functional theory calculations and molecular dynamics (MD) simulations of $LK_7\beta$ at the air−water interface. Irrespective of the handedness of the amino acids, leucine side chains prefer to orient toward the hydrophobic air phase while lysine side chains prefer the hydrophilic water phase. These preferences dictate the backbone configuration of $LK_7\beta$ and thereby the folding of the peptide. Our MD simulations show that the preferred side chain orientations can force the backbone of a single strand of (L-) $LK_7\beta$ at the air−water interface to adopt β-sheet Ramachandran angles. However, denaturation of the β-sheets at pH = 2 results in a negligible chiral VSFG amide I response. The combined computational and experimental results lend critical support to the theory that a chiral VSFG response requires macroscopic chirality, such as in β-sheets. Our results can guide expectations about the VSFG optical responses of proteins and should improve understanding of how amino acid chirality modulates the structure and function of natural and *de novo* proteins at biological interfaces.

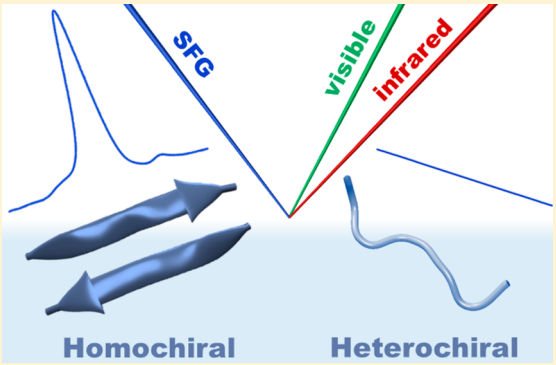

INTRODUCTION

The enantiomeric enrichment of (L-) chirality amino acids placed significant restrictions on the chemical diversity of proteins in the prebiotic world. However, (L-) and (D-) amino acids are occasionally incorporated together in natural systems. For example, the antibiotic peptide gramicidin A consists of 15 alternating (L-) and (D-) amino acids. The peptide adopts the uncommon β-helix-type secondary structure with all side chains on one face of the strand, allowing gramicidin A to function as a membrane cation channel.[1,2] The incorporation of both (L-) and (D-) amino acids in natural proteins requires a complex biosynthetic machinery acting along nonribosomal pathways.[3,4] This raises questions concerning the unique biophysical properties of heterochirality that would justify expanding "Nature's alphabet" to include (D-) amino acids.[5]

(D-) amino acids have been used in the design and synthesis of unnatural proteins.[6−10] Some of the resulting proteins with (D-) amino acids show promise as antiviral and anticancer therapeutic agents, since those unnatural proteins are more resistant to proteolysis, may exchange their chiral recognition in biomolecular interactions, and modulate the biophysical properties of cellular structures.[9,11] For example, the antimicrobial peptide sapesin B composed of only (D-) leucine and lysine has higher antimicrobial activity than all (L-) sapesin B.[12] The improved therapeutic potential has been attributed to distinct interactions between (D-) sapesin B and the cell wall of *Staphylococcus* bacteria. At the molecular level, recent computational work employing all-atom molecular dynamics has systematically studied the impact of mixed (L-) and (D-) chirality on α-helices.[13] The results showed that the (L-) to (D-) chiral inversion of even a single amino acid can locally break the α-helix secondary structure. An outstanding challenge is to understand the perturbations induced by chiral inversion leading to disruption of protein secondary structure.

Vibrational sum frequency generation spectroscopy (VSFG) is a second-order ($\chi^{(2)}$) vibrational spectroscopy that can distinguish between protein secondary structures.[14−23] VSFG is a three-wave mixing process that irradiates the sample with

Received: April 30, 2019
Revised: June 13, 2019
Published: June 13, 2019

Downloaded via YALE UNIV on July 12, 2019 at 21:00:08 (UTC).
See https://pubs.acs.org/sharingguidelines for options on how to legitimately share published articles.

© 2019 American Chemical Society

DOI: 10.1021/acs.jpcb.9b04029
J. Phys. Chem. B 2019, 123, 5769−5781

pulses of visible and IR light with frequencies ω_{vis} and ω_{IR}, respectively, and detects the vibrationally resonant sum frequency response at frequency $\omega_{SFG} = \omega_{vis} + \omega_{IR}$. Due to nonlinear effects of the three-wave mixing process, the VSFG technique is highly sensitive and selective for vibrational probes in anisotropic environments, such as interfaces, and suppresses the background signal from the bulk.[14,18,24−28] When combined with computational modeling, VSFG can provide information on the molecular orientation at interfaces.[27−33] The SFG, visible, and IR beams can each be polarized parallel (p) or perpendicular (s) to the incident plane, yielding eight possible polarization combinations. A comparison of SFG intensities using at least two different polarization combinations can, for example, be used to assess the interfacial orientation of molecules, such as lipid tails and alkyl chains, when probing the CH_3 stretching bands.[29,34−38]

In this paper, we combine achiral and chiral VSFG spectroscopy to probe the perturbations of amino acid chiral inversions on the overall chiral secondary structure of antiparallel β-sheets at interfaces. The experimental data is interpreted through density functional theory (DFT) calculations of the VSFG spectra and protein backbone geometry and bond orientations in molecular dynamic (MD) simulations of the antiparallel β-sheet at the air−water interface. We find that the VSFG technique can distinguish all (L-) or all (D-) antiparallel β-sheets from a variant that contains alternating (L-) and (D-) chirality along the length of the peptide backbone, proving the power of VSFG as a vibrational chiroptical spectroscopy. At the molecular level, we find that the presence of an amphiphilic interface induces a preferential orientation of hydrophobic and hydrophilic amino acid side chains to be exposed to the air or water phases, respectively. These preferred orientations in the peptide sequence of $LK_7\beta$ confine the Ramachandran angles to a β-sheet-like configuration even for a single strand of (L-) $LK_7\beta$, providing an invaluable molecular system to critically examine the chiral SFG theory.[39−42] The mixed (L-)/(D-) chirality conforms to the preferences of side chain orientation and thereby exerts steric constraints that prevent the peptide backbone from forming antiparallel β-sheets. Revealing this novel aspect of how chirality and chemical properties of side chains can modulate the secondary structure and orientation of proteins at interfaces exemplifies the advantages of employing both experiments and theoretical analyses for interpreting the VSFG optical response of peptides and proteins. Moreover, our findings should offer insights into *de novo* design of unnatural proteins with both (L-) and (D-) amino acids with potential applications for engineering interfaces of biomaterials.

METHODS

Sample Preparation. The $LK_7\beta$ (Acetyl-Leu-Lys-Leu-Lys-Leu-Lys-Leu-NH_2, MW: 896.24 g/mol) with all (L-) amino acids was synthesized by GL Biochem Ltd. (Shanghai). The $LK_7\beta$ samples with all (D-) or (L-)/(D-) amino acids (i.e., Acetyl-(L-)Leu-(D-)Lys-(L-)Leu-(D-)Lys-(L-)Leu-(D-)Lys-(L-)Leu-NH_2) were synthesized by AnaSpec, Inc. (Fremont, CA). The lyophilized powder samples were dissolved in deionized H_2O (pH = 7 or pH = 2, HCl adjusted) at 1 mM. The solutions were prepared as 100 μL aliquots, frozen in liquid nitrogen, and stored at −80 °C until use.

For VSFG experiments at the air−glass interface, plain glass microscope slides (Thermo Scientific, Portsmouth, NH; cat. 420-004T, 101616-3) were plasma-cleaned on "high" for 3 min in a plasma cleaner (Harrick Plasma, Ithaca, NY; PDC-32G). One aliquot of the $LK_7\beta$ was thawed and pipetted onto the glass slides. The samples dried overnight at room temperature, forming hydrated thin-films at the air−glass interface.

For VSFG experiments at the air−water interface, 200 μL of 1 mM $LK_7\beta$ solution was applied with a glass syringe (Hamilton Company, Reno, NV; model 1705N) at the surface of 3.8 mL of deionized water, giving a final concentration of $LK_7\beta$ of 50 μM.

VSFG Measurements. The VSFG spectra were collected with a home-built setup previously described.[43] For achiral VSFG measurements, we centered the broad-band IR beam at 3300 nm and used the *ssp* polarization configuration (*s*-polarized sum frequency, *s*-polarized visible, and *p*-polarized IR). For chiral amide I/amide II VSFG measurements, we centered the broad-band IR beam at 6100 nm and used the *psp* polarization configuration. Spectra taken at the air−glass interface were collected with acquisition times of 10 min (unless otherwise noted). Spectra taken at the air−water interface were collected with acquisition times of 20 min.

The reported IR frequencies are recovered by calibrating the VSFG response to a polystyrene standard (Buck Scientific, East Norwalk, CT, USA; 0.05 mm film). Background spectra were collected by shuttering the IR beam. The background spectra were then subtracted from the VSFG intensity spectra. For VSFG spectra at the air−glass and air−water interfaces, the background-subtracted spectra were normalized to the IR power envelope by dividing by the VSFG response of a GaAs crystal. The VSFG spectra were manually cleaned of cosmic ray intensities, which are unrelated to the VSFG response.

Finally, the intensity spectra were fit to a Lorentzian function that describes the resonant vibrational mode being probed and a contributing nonresonant term

$$I_{SFG} \propto \left| \chi^{(2)}_{NR} + \sum_q \frac{A_q}{\omega_{IR} - \omega_q + i\Gamma_q} \right|^2 \quad (1)$$

where I_{SFG} is the intensity of the sum frequency generation, $\chi^{(2)}_{NR}$ is the nonresonant second-order susceptibility, ω_{IR} is the frequency of the IR beam, A_q is the amplitude of the qth resonant vibrational mode, ω_q is the frequency, and Γ_q is the half-width half-maximum.

Molecular Dynamics. Molecular dynamics simulations of all (L-), all (D-), and (L-Leu)/(D-Lys) $LK_7\beta$ on the water/air interface were performed using the all-atoms CHARMM36/CMAP force field[44] and the TIP3P water model potential.[45] The force field parameters for the (D-) amino acids were taken from the residue topology 'toppar_all36_prot_d_amino acids.str' that includes inverted CMAP tables from the corresponding (L-) amino acids. All simulations were performed using the NAMD software package[46] in the NVT ensemble using a Langevin thermostat with a time constant of 1 ps. Hydrogen bonds were kept fixed using the SETTLE algorithm,[47] which allows the use of a 2 fs time step. Periodic boundaries conditions in three dimensions were applied using a cutoff of 12 Å for the real-space Coulombic and van der Waals interactions, whereas long-range interactions were handle using the particle-mesh Ewald method (PME).

The initial LK_7 polypeptides strands were built in the β-conformation by tacking backbone dihedral angles (ϕ, ψ) of (−120, 113) for L-amino acids and (120, −113) for D-amino acids, using the Molefacture plugin in the VMD package.[48]

DOI: 10.1021/acs.jpcb.9b04029
J. Phys. Chem. B 2019, 123, 5769−5781

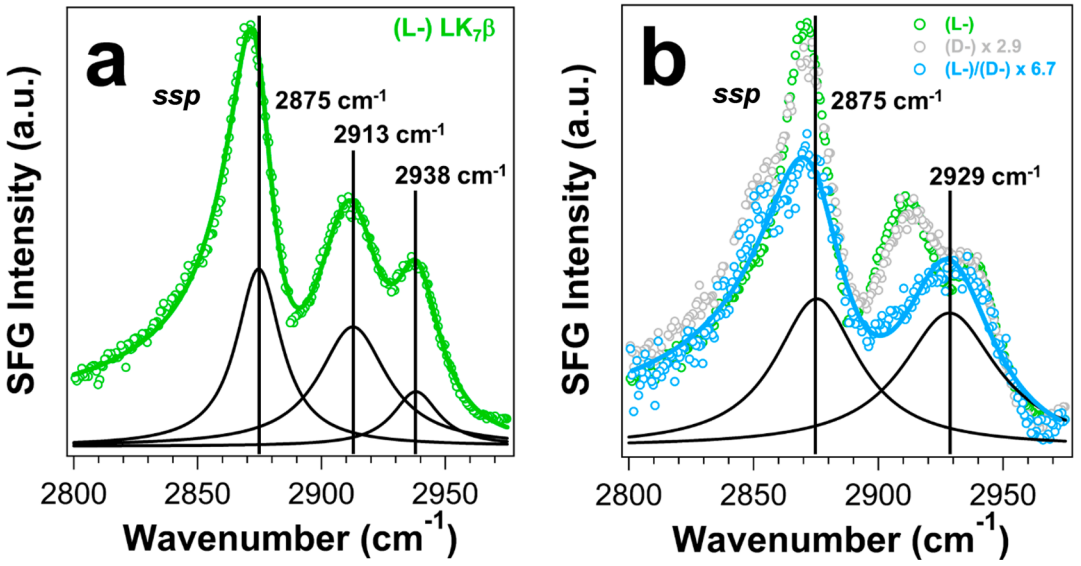

Figure 1. VSFG of (L-), (D-), and (L-Leu)/(D-Lys) LK$_7\beta$ at the air−water interface in the C−H stretching region. The spectra of (L-) and (D-) LK$_7\beta$ show identical profiles whereas the (L-Leu)/(D-Lys) variant shows strong suppression of the peak at 2913 cm^{-1}. The spectra are measured using the *ssp* (achiral) polarization combination. Solid colored lines are fits to the spectra based on eq 1. Solid black lines are the component peaks of the fits.

The side chains of the lysine residues were taken to be charged. The N-terminal and C-terminal of the polypeptide chains were capped with $-NH_2COCH_3$ (acetylated N-terminus) and $-CONH_2$ (amidated C-terminus) groups, respectively. From these polypeptide strands, β-sheets were assembled in antiparallel conformation using 2 strands.

The β-sheets were placed on the surface of a pre-equilibrated TIP3P water slab with the hydrophobic leucine residues facing the air. The water slab consists of 4855−4893 water molecules arranged in a ∼35 Å thick slab of 70 × 70 Å^2 surface area, with ∼35 Å of vacuum in the direction perpendicular to the slab (defined as the z direction). In order to maintain charge neutrality, random waters were replaced by Cl^- atoms. The combined protein−water system was allowed to relax using a conjugate gradient algorithm for 5000 steps to eliminate any close contact interaction between atoms, followed by an 820 ps simulation where the system was heated from 30 to 298 K. An additional 400 ps simulation at 298 K was carried out to equilibrate the system at the target temperature. For all (L-) and all (D-) LK$_7\beta$, a 20 ns production simulation was used to extract dihedral angles and angular distribution using snapshots every 1 ps. For (L-Leu)/(D-Lys) LK$_7\beta$, longer simulations of 60 ns were performed. Results for the all (L-) and all (D-) LK$_7\beta$ correspond to averages over three independent simulations with different initial configurations, whereas results for the (L-Leu)/(D-Lys) LK$_7\beta$-model correspond to averages over five simulations.

Calculation of VSFG Spectra. VSFG spectra were computed for an antiparallel β-sheet model composed of two LK$_3$ peptides, with the primary sequence Leu-Lys-Leu. This peptide represents a minimal model with the characteristics of the LK$_7\beta$ peptide. Geometry optimizations and harmonic frequency analysis at the DFT level were performed with the Gaussian 2009 software package,[49] using the B3LYP[50] hybrid functional and the 6-31G(d) basis set.[51] An "ultrafine" integration grid (99 radial shells and 590 angular points per shell) was used for the frequency calculations to obtain accurate results.

Our approach for simulating SFG spectra has been previously described.[17,20,52−58] Here, we describe it only briefly. The calculations involve the determination of the second-order molecular hyperpolarizabilities $\beta^{(2)}_{ijk,q} \propto \frac{\partial \alpha_{ij}}{\partial Q_q} \cdot \frac{\partial \mu_k}{\partial Q_q}$, where α_{ij} and μ_k (with i, j, k = a, b, c) are elements of the polarizability and dipole moment in the molecular frame, respectively, and Q_q is the normal coordinate of the qth vibrational mode. The hyperpolarizability $\beta^{(2)}_{ijk,q}$ is then rotated to the laboratory frame (x, y, z) and averaged over the azimuthal angle ϕ in 5° increments to obtain the second-order susceptibility $\chi^{(2)}_{IJK,q} = \sum_{ijk}\langle R_{Ii}\cdot R_{Jj}\cdot R_{Kk}\rangle \cdot \beta^{(2)}_{ijk,q}$, where R_{Ii} represent elements of the ZYZ Euler rotation matrix.[18] The susceptibilities $\chi^{(2)}_{IJK,q}$ are then used to compute the effective susceptibilities, which for the *ssp* and *psp* polarization combinations take the form[18,27,29]

$$\chi^{(2)}_{ssp,q} = L_{yyz}\chi^{(2)}_{yyz,q} \tag{2}$$

$$\chi^{(2)}_{psp,q} = L_{zyx}\chi^{(2)}_{zyx,q} - L_{xyz}\chi^{(2)}_{xyz,q} \tag{3}$$

where L_{yyz} terms represent Fresnel factors that depend on the refractive index of the interface as well as the incident angle of the lights.[18,27,29] The Fresnel factors used in this study are listed in Table S2. From these susceptibilities, the homodyne SFG spectra are given by

$$I_{SFG}(\omega_{IR}) \propto |\chi^{(2)}|^2 = \left| A_{NR}e^{i\phi} + k\sum_q \frac{\chi^{(2)}_q}{\omega_{IR} - \omega_q + i\Gamma_q} \right|^2 \tag{4}$$

where k is a multiplicative constant. All harmonic frequencies were scaled by 0.943 to facilitate comparisons with experiments whereas Γ_q and A_{NR} were set to 7.5 cm^{-1} and 0, respectively.

DOI: 10.1021/acs.jpcb.9b04029
J. Phys. Chem. B 2019, 123, 5769−5781

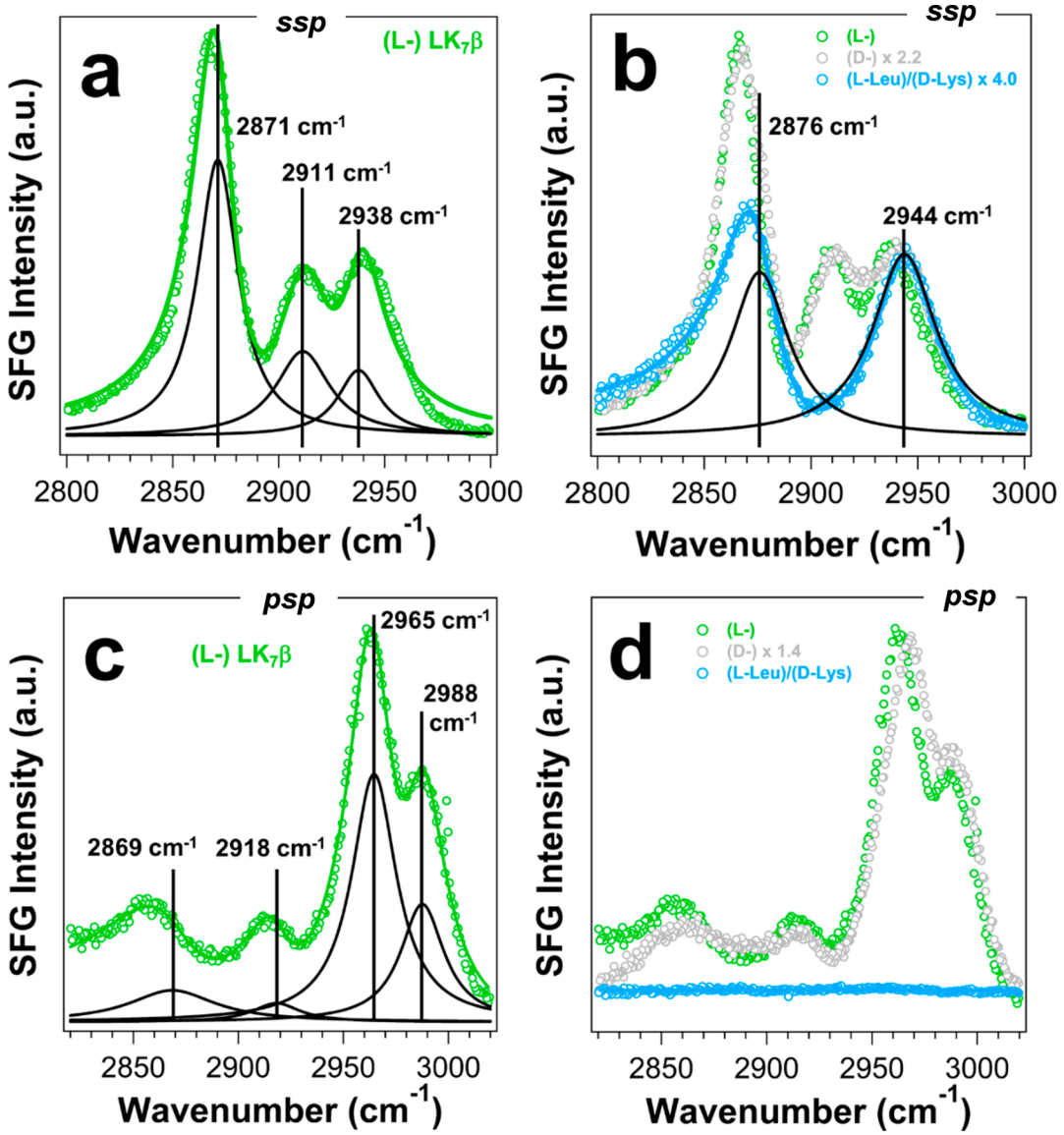

Figure 2. VSFG of (L-), (D-), and (L-Leu)/(D-Lys) LK$_7\beta$ at the air−glass interface in the C−H stretching region. Similar to the air−water interface, the peak at 2911 cm^{-1} is suppressed in the (L-Leu)/(D-Lys) variant. The spectra in parts a and b are measured using the *ssp* (achiral) polarization combination. The spectra in parts c and d are measured with the *psp* (chiral) polarization combination. Solid colored lines are fits to the spectra based on eq 1. Solid black lines are the component peaks of the fits.

RESULTS

Achiral and Chiral VSFG of (L-), (D-), and (L-Leu)/(D-Lys) LK$_7\beta$. We previously demonstrated by VSFG amide I response that the (L-) LK$_7\beta$ peptide spontaneously forms antiparallel β-sheets at interfaces.[54] The LK$_7\beta$ peptide localizes to the air−water interface due to alternating hydrophobic leucine and hydrophilic lysine residues.[59] Figure 1 shows the achiral (*ssp*) VSFG spectra of (L-), (D-), and (L-Leu)/(D-Lys) LK$_7\beta$ variants at the air−water interface. The (L-) LK$_7\beta$ shows three peaks in the C−H stretching region (Figure 1a) in agreement with the spectrum reported by Somorjai and co-workers.[60] The peaks are centered at 2875, 2913, and 2938 cm^{-1}. Their assignments are aided by computational studies as discussed in the next section (Computations of VSFG Spectra). The (L-) LK$_7\beta$ and (D-) LK$_7\beta$ spectra are indistinguishable (Figure 1b, green and gray). However, the achiral VSFG spectrum for (L-Leu)/(D-Lys) LK$_7\beta$ is distinguished by significant suppression of the peak at 2913 cm^{-1} (Figure 1b, blue). Suppression of this peak is also observed at the air−glass interface (Figure 2a,b). In contrast, linear vibrational spectroscopy such as attenuated total reflectance-Fourier transform infrared does not distinguish between the three LK$_7\beta$ species in the C−H stretching region (Figure S1, Section S1 in Supporting Information).

We also probed LK$_7\beta$ variants at the air−glass interface using chiral (*psp*) VSFG, which is sensitive to anisotropic orientation of local chiral moieties as well as macroscopic chirality.[23,41,42] The chiral VSFG response can report on the formation of higher-order chiral structures of biological macromolecules, for example, α-helix or β-sheet secondary structure of proteins and hybridization of double-helix DNA.[19,23,61] The (L-) LK$_7\beta$ peptide shows at least four peaks in the C−H stretching region (Figure 2c), in agreement with our prior report of chiral VSFG spectra of LK$_7\beta$ at the air−water interface.[62] The peak positions, centered at 2869, 2918, 2965, and 2988 cm^{-1}, were previously assigned to the CH$_3$

DOI: 10.1021/acs.jpcb.9b04029
J. Phys. Chem. B 2019, 123, 5769−5781

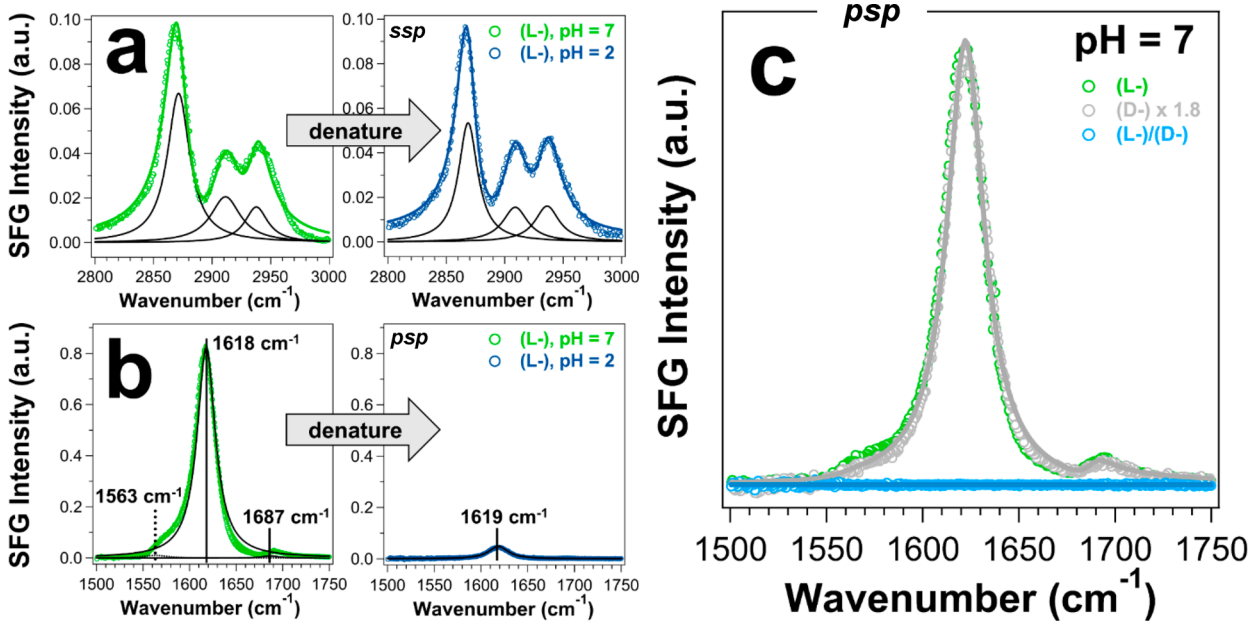

Figure 3. Achiral and chiral VSFG of LK$_7\beta$ at the air−glass interface prepared using native pH = 7 and denaturing pH = 2 conditions. (a, b) Loss of antiparallel β-sheet structure at pH = 2 induces a loss of chiral amide I/amide II signal, which is not correlated with suppression of the C−H stretching peak at 2913 cm^{-1}. (c) (L-Leu)/(D-Lys) LK$_7\beta$ does not show a chiral VSFG signal in the amide I/amide II region. The spectra in part a are measured using the *ssp* (achiral) polarization combination. The pH = 2 spectra in part a was scaled by 2×. The spectra in parts b and c are measured with the *psp* (chiral) polarization combination.

symmetric stretch, CH_2 asymmetric stretch, CH_3 asymmetric stretch, and C_α−H stretching modes, respectively.[62] The (D-) LK$_7\beta$ spectrum is very similar and overall indistinguishable (Figure 2d, green and gray). In contrast, a chiral response for (L-Leu)/(D-Lys) LK$_7\beta$ was not observed (Figure 2d, blue). These observations suggest that (L-Leu)/(D-Lys) LK$_7\beta$ at the air−glass interface neither assumes a configuration in which local chiral moieties produce a coherent VSFG response nor adopts a chiral secondary structure.

We have also analyzed the effect of pH by preparing (L-) LK$_7\beta$ at the air−glass interface at neutral pH = 7 and denaturing pH = 2. We find that the peak at 2913 cm^{-1} is clearly not suppressed at pH = 2 (Figure 3a). Furthermore, we measured the chiral amide I/amide II response of (L-) LK$_7\beta$ at the air−glass interface at both pH = 7 and pH = 2. We have previously shown that the chiral amide I response is a useful probe of the protein secondary structure at interfaces.[16,18] For LK$_7\beta$, the peaks at 1563, 1618, and 1687 cm^{-1} are assigned to the amide II, amide I (B_2), and amide I (B_1) vibrational modes associated with antiparallel β-sheets, respectively (Figure 3b, left).[18,54] However, the chiral amide I/amide II spectrum measured with the *psp* polarization is almost completely abolished at pH = 2 (Figure 3b, right). This suggests that the antiparallel β-sheet character of the peptide is mostly lost under denaturing conditions. Altogether, these results show that the loss of antiparallel β-sheet structure is not correlated with suppression of the peak at 2913 cm^{-1} as observed for the (L-Leu)/(D-Lys) LK$_7\beta$ spectrum (Figures 1b and 2b). Finally, Figure 3c shows the chiral amide I/amide II spectrum measured for the different LK$_7\beta$ variants at pH = 7. The (L-) and (D-) LK$_7\beta$ spectra show a strong chiral response, while no VSFG signal is observed for (L-Leu)/(D-Lys) LK$_7\beta$.

The suppression of the VSFG response of the resonant vibrational mode at 2913 cm^{-1} for (L-Leu)/(D-Lys) LK$_7\beta$ (Figures 1 and 2) and our finding that the suppression of this mode is not correlated with loss of antiparallel β-sheet structure (Figure 3) prompt some interesting questions. What is the identity of the vibrational normal mode at 2913 cm^{-1}? Why is this mode suppressed in heterochiral versus homochiral LK$_7\beta$ variants? How do chiral inversions inhibit or promote protein secondary structure at interfaces? To address these research questions in molecular detail, we used DFT to recapitulate the VSFG response of (L-) LK$_7\beta$. We also performed MD simulations to understand the effects of chiral inversions on protein secondary structure and side chain dynamics of (L-), (D-), and (L-Leu)/(D-Lys) LK$_7\beta$ at the air−water interface.

Computations of VSFG Spectra. To approximate the VSFG response of (L-) LK$_7\beta$ and assign the peak at 2913 cm^{-1}, we performed DFT calculations on an antiparallel β-sheet model composed of two (L-) LK_3 peptides with primary sequence Ac-Leu-Lys-Leu-NH_2 (Figure 4a). The model peptide represents a minimal "building block" with the characteristics of (L-) LK$_7\beta$ amenable to *ab initio* calculations. While treatments based on second-order perturbation theory (VPT2)[63−66] or vibrational self-consistent field (VSCF)[67−69] methods are available to include overtones and combination bands in the description of the spectra, the dimension of the system under consideration makes such calculations infeasible. Nevertheless, we find that an anharmonic analysis comprising Fermi resonances (FRs) on single leucine and lysine residues including couplings between modes[70−72] is sufficient for understanding the C−H stretch spectral region (Section S2 in Supporting Information).

Figure 4b shows the calculated *ssp* VSFG spectrum of the antiparallel β-sheet model for a molecular orientation with the *c*-axis perpendicular to the surface plane (axis coordinates are shown in Figure 4a). This orientation exposes the hydrophobic leucine side chains to the hydrophobic phase and the charged lysine side chains to the hydrophilic phase. This is the

DOI: 10.1021/acs.jpcb.9b04029
J. Phys. Chem. B 2019, 123, 5769−5781

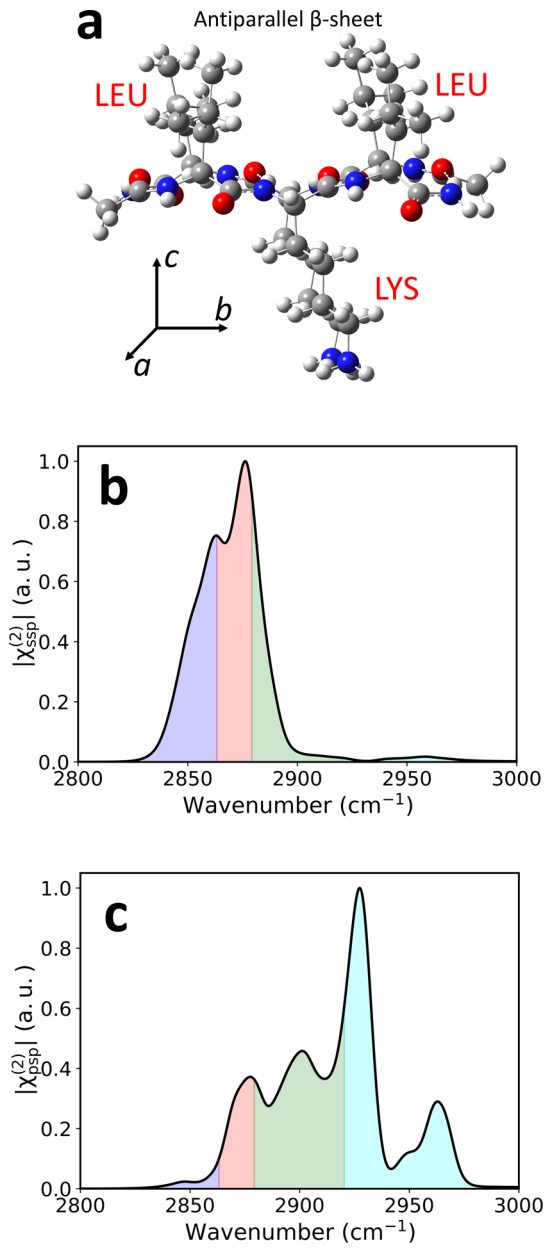

Figure 4. (a) Molecular representation of the antiparallel β-sheet all (L-) $(LK_3)_2$ model peptide, defined in the molecular frame *a*, *b*, *c*. DFT-based (b) *ssp* and (c) *psp* SFG spectra. Shaded areas correspond to symmetric CH_2 (purple), symmetric CH_3 (red), asymmetric CH_2 (green), and asymmetric CH_3 (cyan) stretching modes.

dominant structure of the antiparallel β-sheet at the air−water interface (see next section). The spectrum is characterized by a broad peak centered at 2875 cm^{-1} attributed to the symmetric CH_3 stretching (normal-mode analyses are presented in Section 3 in Supporting Information). This peak has shoulders at both sides due to symmetric and asymmetric CH_2 stretching (note that a shoulder possibly appears around 2850 cm^{-1} in the experimental spectrum in Figure 1). On the basis of this analysis, the peak at 2875 cm^{-1} in the experimental spectra in Figures 1 and 2 can be assigned to the symmetric CH_3 stretch. Allowing for the contributions of FRs of the symmetric CH_3 and CH_2 stretching of leucine and lysine side chains (Supporting Information) and given the strong intensity of the symmetric CH_3 and CH_2 peaks, from which intensity of the FR is borrowed, we assign the experimental peak at 2913 cm^{-1} to the FR of the symmetric CH_2 stretching and the peak at 2938 cm^{-1} to CH_3 FR. The lysine C_α−H is coupled to the CH_2 FRs and possibly also contributes in the experimental spectrum. This assignment, based on DFT calculations, is in agreement with previous studies of the $LK_7\beta$ polypeptide as well as individual leucine and lysine residues.[22,33,60,73−75] It should be noted that the symmetric CH_3 stretching band of the capping group appears at ∼2893 cm^{-1} and might also contribute to the spectral signals. We cannot presently discard the contribution of this capping group to the experimental spectra. However, the reasonable agreements in peak position and relative intensity between the calculated and experimental spectra, as well as previous SFG studies of $LK_7\beta$ and related systems such as $LK_{14}\alpha$, leucine, and lysine amino acids,[22,33,60,73−77] suggest that the contribution of the capping to the SFG signal should be small.

In Figure 4c, we present the chiral spectra for the model peptide. The simulated and experimental spectra (Figure 2c) agree very well. The spectra consist of four bands, including symmetric CH_3, asymmetric CH_2, asymmetric CH_3, and C_α−H stretching modes.[62] As noted above, the asymmetric CH_2 stretching modes that appear in the region 2900−2930 cm^{-1} are highly coupled to the chiral C_α−H of the lysine residues. The higher-frequency peaks comprise the stretching of the leucine chiral C_α−H moieties (with some possible overlap with the asymmetric CH_3 stretching of the acetyl capping group). For the spectrum in Figure 4c, it is difficult to assess the effects of FRs in the chiral SFG signal. Further studies are required.

Molecular Dynamics and Orientation Analysis of (L-), (D-), and (L-Leu)/(D-Lys) $LK_7\beta$. To obtain molecular detail on the interfacial behavior of the $LK_7\beta$ system, we complement the VSFG experiments and calculations with MD simulations. The simulated systems consist of a water slab with (L-), (D-), or (L-Leu)/(D-Lys) $LK_7\beta$ placed at the air−water interface (Figure 5).

We first characterize the backbone conformation of polypeptides with different chiralities by computing free energy profiles along the backbone dihedral angles ϕ and ψ. In Figure 6a, we present the free energy profile for (L-) $LK_7\beta$ composed of two strands in an antiparallel β-sheet conformation at the air−water interface. The free energy landscape presents a well spanning the region $-160° < \phi < -80°$ and $100° < \psi < 150°$, characteristic of β-sheet conformations.[78] An analysis of the free energy profile per residue (Figure S5) also corroborates the presence of β-sheet conformations. In this conformation all the hydrophilic lysine residues are placed on one side of the sheet and are solvated by the water phase; all the hydrophobic leucine residues point into the air (Figure 5a). In fact, a simulation test in which the $LK_7\beta$ is started with the leucine residues pointing into the water and the lysine residues into the air shows that the system naturally evolves to invert the orientations of the residues (Figure S7).

Figure 6b shows the Ramachandran free energy profile for a two-strand (D-) $LK_7\beta$ system. The free energy landscape obtained for this system is a mirror image of the one for the (L-) $LK_7\beta$ (Figure 6a), and it represents the β-sheet conformational region for (D-) amino acids.[78]

We found that a system of two strands of (L-Leu)/(D-Lys) $LK_7\beta$ does not form stable antiparallel β-sheets as the strands break apart over the course of the simulation (Figure S8, Section 6 in Supporting Information). Indeed, previous

DOI: 10.1021/acs.jpcb.9b04029
J. Phys. Chem. B 2019, 123, 5769−5781

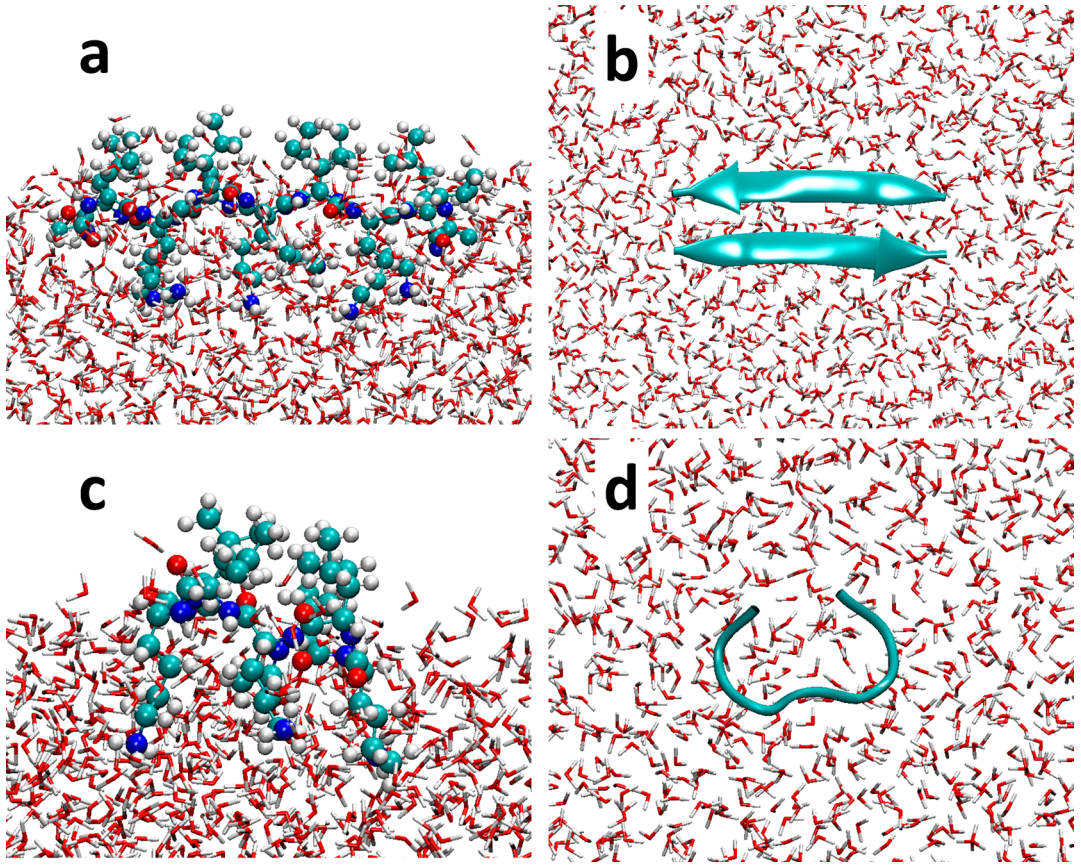

Figure 5. Typical snapshots of the molecular dynamics simulations of LK$_7\beta$ at the air−water interface. (a, b) Side view and top view of (L-) LK$_7\beta$. (c, d) Side view and top view of (L-Leu)/(D-Lys) LK$_7\beta$.

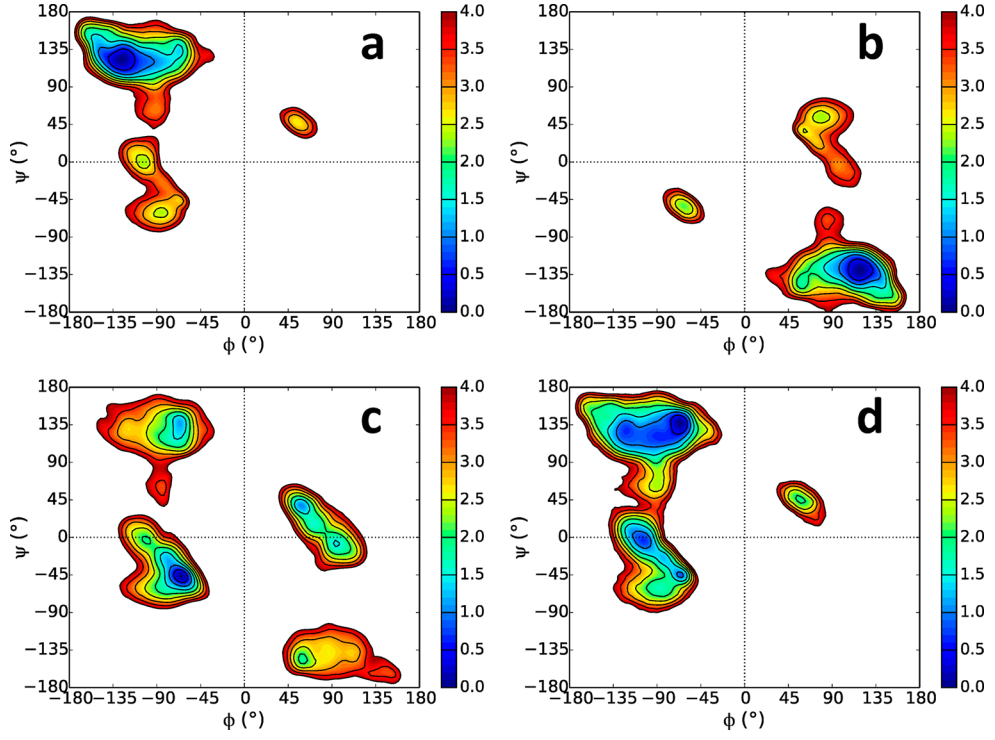

Figure 6. Free energy (k_BT units) as a function of the dihedral angles ϕ and ψ for (a) (L-) (two-strands), (b) (D-) (two-strands), (c) (L-Leu)/(D-Lys) (one-strand), and (d) (L-) (one-strand) LK$_7\beta$.

DOI: 10.1021/acs.jpcb.9b04029
J. Phys. Chem. B 2019, 123, 5769−5781

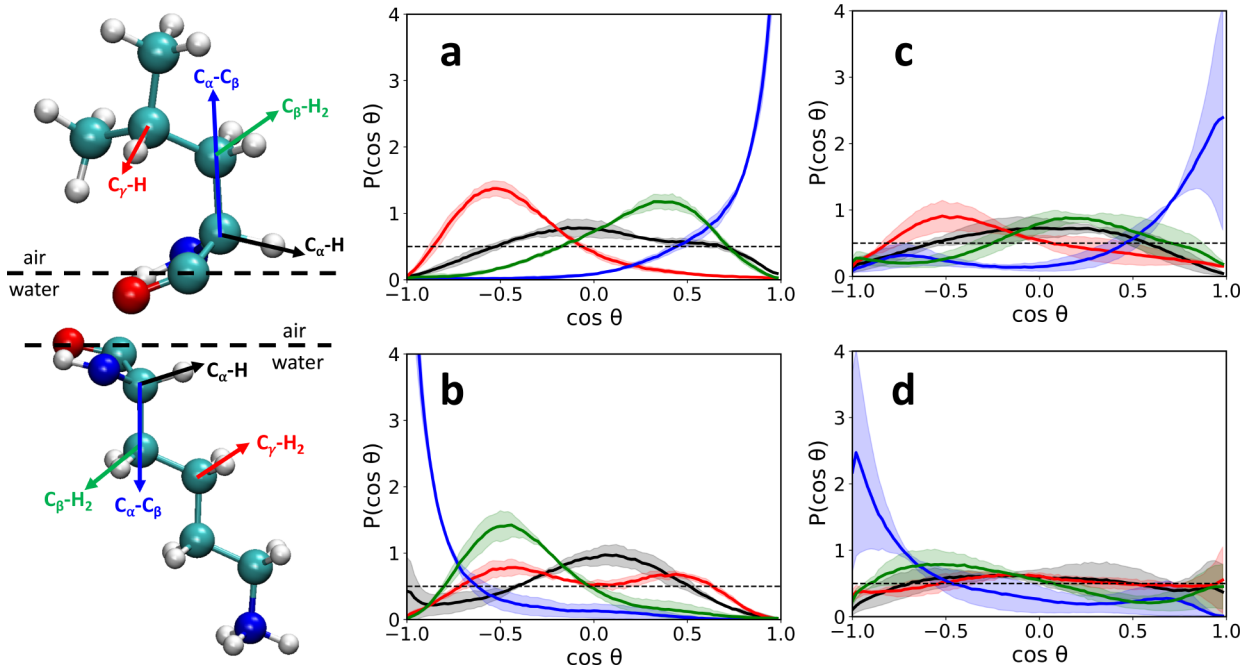

Figure 7. (Left) Schematic representation of leucine (top) and lysine (bottom) residues with colored definition of bond vectors used to describe the orientation with respect to the surface normal. Angular distributions of selected bond vectors of leucine (a) and lysine (b) for (L-) LK$_7\beta$. Angular distributions of selected bond vectors of leucine (c) and lysine (d) for (L-Leu)/(D-Lys) LK$_7\beta$. Shaded areas correspond to the standard deviation of the distributions. Dashed lines correspond to an isotropic distribution of the angles.

experimental and computational studies showed that inversion of chirality at a particular placement along a peptide chain leads to a consequent break in secondary structure.[13,78−83] Our MD results also suggest that the (L-Leu)/(D-Lys) LK$_7\beta$ species do not form any stable secondary structure, consistent with the VSFG silent chiral amide I/amide II spectrum (Figure 3c). Hence, for the (L-Leu)/(D-Lys) LK$_7\beta$ we only present results obtained with one polypeptide strand (Figure 5c,d). Figure 6c shows the free energy profile for the one-strand (L-Leu)/(D-Lys) LK$_7\beta$ system. The free energy landscape is richer and more complicated than for the (L-) or (D-) LK$_7\beta$ variants and demonstrates a more complex behavior of the polypeptide, which dynamically samples various configurations over the course of the simulation (Figure S6). The periodic alternation of chirality in the (L-Leu)/(D-Lys) LK$_7\beta$ system represents a huge perturbation in the "natural" behavior of the polypeptide, not allowing for the formation of local secondary structure motifs.

To further highlight the effect of chiral inversion on the dynamics and structure of peptides, we also performed simulations of a single strand of (L-) LK$_7\beta$ on the air−water interface. Upon comparison of this system with the (L-Leu)/(D-Lys) LK$_7\beta$ and the two strands of (L-) LK$_7\beta$, it is possible to disentangle the effect of chiral inversion from the absence of a β-sheet. The free energy profile of the backbone for this system is presented in Figure 6d. The conformation adopted by the single strand of (L-) LK$_7\beta$ does not present such a complex landscape as the one adopted by the (L-Leu)/(D-Lys) LK$_7\beta$ (see also Figure S6), demonstrating that the inversion in chirality has a more profound effect than just disrupting the secondary structure of the peptide. Quite remarkably, while the one isolated strand of (L-) LK$_7\beta$ displays a richer landscape than for the system with two strands (Figure 6a), the single strand is predominantly characterized at the air−water interface by a stable backbone geometry consistent with β-strand conformation. Since it is not possible to form interstrand hydrogen bonds, the single strand must be stabilized by the interface itself. Indeed, the hydrophobic leucine side chains continue to point toward the air phase, while the hydrophilic lysine residues point toward the water phase (Figures S9 and S10).

The Ramachandran free energy plots presented in Figure 6 are informative with respect to the effect of chirality on the conformation of the peptide backbone but do not give information on the orientation of the side chains with respect to the interface, which is the information gathered from achiral VSFG spectra.[18] To characterize the behavior of the side chains we computed the tilt angle (θ) of certain bonds with respect to the surface normal. A schematic representation of the representative selected bonds is presented in Figure 7.

In Figure 7a we present the tilt angle distributions over all the leucine residues for two strands of (L-) LK$_7\beta$. Average values and standard deviations for tilt angles obtained from these distributions are presented in Table S1. The angle θ of the C_α−C_β bonds (blue) presents a peaked distribution with a maximum near 0° ($\cos\theta = 1$), which demonstrates the extreme preference of leucine hydrophobic side chains to point toward the air. The tilt orientation of C_α−H bonds (black) presents a broad distribution centered around $\theta = 90°$ ($\cos\theta \approx 0$) and is consistent with the formation of antiparallel β-sheets with hydrogen bonds between C═O···H−N lying on the plane of the water surface (Figure S11). The isopropyl group of leucine residues, characterized by the C_γ−H bond (red), presents a broad distribution centered around 120° ($\cos\theta \approx -0.52$), implying a strong ordering at the interface as suggested by previous studies.[19,33,60,74,84−86] Note that since the principal peaks at 2875 and 2938 cm^{-1} of the *ssp* SFG spectra in the C−H stretch region are ascribed to the methyl groups of the leucine residue (symmetric stretching and FR, respectively), the peaked distribution of C_γ−H supports the presence of an

DOI: 10.1021/acs.jpcb.9b04029
J. Phys. Chem. B 2019, 123, 5769−5781

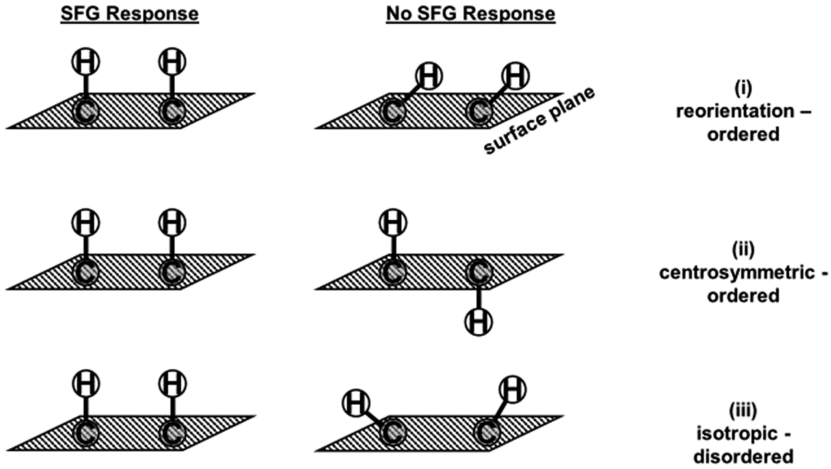

Figure 8. Conditions for an inactive VSFG signal. For the purpose of example in the cases outlined, it is assumed that the transition dipole moment points parallel to the bond.

SFG-active ordered interface. The θ distributions for (D-) LK$_7\beta$ are essentially the same compared to the results for (L-) LK$_7\beta$ (Figure S9).

The distributions of the tilt angles over all the lysine residues in (L-) LK$_7\beta$ are presented in Figure 7b. The lysine side chains preferentially face the water phase, as can be appreciated from the peak C_α–C_β distribution (blue) at θ = 180°. The distribution of C_α–H angles (black) is centered at θ = 90° consistent with the formation of antiparallel β-sheets. The $C_\beta H_2$ moiety (green) is ordered. Note that the distribution of the $C_\gamma H_2$ moieties (red) is bimodal, with peaks at $\theta \approx 120°$ ($\cos\theta \approx -0.47$) and $\theta \approx 65°$ ($\cos\theta \approx 0.40$). This implies that the alkyl chains are not fully ordered in perfect *trans* conformation and present some *gauche* defects, consistent with their VSFG optical activity.[35] Again, the θ distributions for (D-) LK$_7\beta$ are unchanged (Figures S10 and S11).

The results for the tilt angle for one strand of (L-Leu)/(D-Lys) LK$_7\beta$ peptide are presented in Figure 7c,d. The leucine and lysine side chains still point up and down, respectively, maintaining the tendency of hydrophobic or hydrophilic residues to point into the air or water phase (blue curves). The biggest contrasts with (L-) LK$_7\beta$ are the distributions of lysine $C_\gamma H_2$ and C_α–H (Figure 7d, red and black curves). Both distributions become nearly isotropic, indicating that these modes should not be observed in a VSFG experiment.

DISCUSSION

To the best of our knowledge, there have been no reports of VSFG being applied to study the effects of mixed (L-)/(D-) chirality on protein secondary structure. Here, we used achiral and chiral VSFG in combination with computational studies of protein dynamics to investigate biophysical properties of (L-Leu)/(D-Lys) LK$_7\beta$ at interfaces. We now provide an explanation for the achiral and chiral VSFG optical responses of (L-), (D-), and (L-Leu)/(D-Lys) LK$_7\beta$ variants, and relate chiral inversions of the peptide backbone with protein secondary structure and side chain dynamics.

Identical Achiral VSFG Spectra of (L-) and (D-) LK$_7\beta$. The achiral VSFG spectra of (L-) and (D-) LK$_7\beta$ show strong resonant responses in the C–H stretching region around 2875, 2913, and 2938 cm^{-1} (Figures 1a and 2a). Our harmonic DFT frequency calculations of a model peptide, supplemented with anharmonic calculations of single amino acids, suggest assigning these peaks to the leucine CH_3 symmetric stretch, Fermi resonance modes arising from the CH_2 symmetric stretching (with possible contributions from lysine C_α–H stretching and CH_3 symmetric stretch of the N-terminal acetyl cap), and leucine symmetric CH_3 Fermi resonance, respectively, in agreement with previous studies.[22,33,60,73−75] The spectral responses of (L-) and (D-) LK$_7\beta$ in the C–H stretching region are identical, suggesting that a total inversion of the chirality of the amino acids does not affect the properties of the LK$_7\beta$ at the interface. These results are confirmed by molecular dynamics simulations demonstrating that both the distribution of backbone dihedral angles (Figure 6) as well as the orientations of side chains (Figures S7 and S8) are identical for the (L-) and (D-) LK$_7\beta$ peptide at the air–water interface.

Silent CH_2 Fermi Resonance Vibration in VSFG of (L-Leu)/(D-Lys) LK$_7\beta$. When the LK$_7\beta$ peptide is formed by an alternation of (L-Leu) and (D-Lys) amino acid residues, the vibrational mode at 2913 cm^{-1} in the achiral VSFG spectrum is silenced, although the vibrational modes at 2875 and 2938 cm^{-1} still show (Figures 1b and 2b). This is especially intriguing given that linear, non-surface-selective spectroscopy such as ATR-FTIR (Figure S1) hardly distinguishes among the (L-), (D-), and (L-Leu)/(D-Lys) LK$_7\beta$ variants in the C–H stretching region.

In general, three possible conditions can lead to a silent achiral VSFG signal (Figure 8). (i) The molecular system adopts an ordered orientation that is VSFG inactive due to the polarization combination used in the experiment and, consequently, the selection rules over $\chi^{(2)}$. For example, the transition dipole moment might be perpendicular to the applied electric field of the linearly polarized IR beam. (ii) The molecular system adopts an ordered centrosymmetric orientation around the interface resulting in a (destructive) interference between vibrational modes and a null mean second-order polarizability, $\overline{P}^{(2)} = 0$. (iii) The molecular system adopts a disordered, isotropic orientation around the interface, resulting in $\overline{P}^{(2)} = 0$. In order to understand why the lysine CH_2 2913 cm^{-1} peak is absent in the achiral VSFG spectrum of (L-Leu)/(D-Lys) LK$_7\beta$, it is necessary to determine which of the three conditions is responsible for the silent VSFG signal. This required a combination of experimental and computational research, including DFT calculations of VSFG spectra and MD simulations.

DOI: 10.1021/acs.jpcb.9b04029
J. Phys. Chem. B 2019, 123, 5769−5781

Scenario i: Reorientation. Our Ramachandran analyses (Figure 6c and Figure S6) show that (L-Leu)/(D-Lys) LK$_7\beta$ does not form stable β-sheets, but dynamically samples different conformations. On the other hand, the analysis of the orientation of CH_2 groups of the lysine side chain (Figure 7d) shows no apparent net orientation for this group. These results allow us to rule out scenario i, namely, that (L-Leu)/(D-Lys) LK$_7\beta$ at the interface adopts an *ordered* conformation that is differently oriented and thus VSFG inactive.

Scenario ii: Centrosymmetric Order. A similar analysis of our simulations also let us exclude scenario ii, a centrosymmetric ordering at the interface. The Ramachandran free energy plot of (L-Leu)/(D-Lys) LK$_7\beta$ certainly demonstrates that the peptide backbone lacks secondary structure at the interface (Figure 6c). Moreover, the analysis of the orientation of lysine side chains does not show an alternate orientation of CH_2 groups that might lead to a destructive interference of vibrational modes. However, achiral VSFG reports not only on the absence or presence of protein secondary structure but is convoluted with the vibrational modes of local chemical groups. This means that the free energy landscape of the peptide backbone structure is not enough to rule out all kinds of conformational order at the interface that could contribute to (or silence) the VSFG response. Therefore, when analyzing achiral VSFG data it should be necessary to understand local bond tilt angle distributions as we have done in this work (Figure 7).

Scenario iii: Isotropic Dynamics. Our bond tilt angle analyses show that the introduction of chiral inversions at the lysine positions result in lysine C_α−H and $C_\gamma H_2$ being isotropic (Figure 7d), while the orientation of leucine side chains is not much affected by chiral inversion (Figure 7c). From this, we conclude that it is the isotropic nature of the coupled lysine C_α−H and CH_2 groups in (L-Leu)/(D-Lys) LK$_7\beta$ that silences the response at 2913 cm^{-1}, compared to the achiral VSFG spectra of (L-) LK$_7\beta$ and (D-) LK$_7\beta$ at interfaces.

Side Chain Preferences Dominate Protein Secondary Structure at Interfaces. The structural free energy landscape of the peptide backbone of (L-Leu)/(D-Lys) LK$_7\beta$ shows multiple minima (Figure 6c) that are dynamically sampled by the peptide (Figure S6). This behavior might simply be attributed to the lack of interstrand hydrogen bonding. However, our simulations show that even a single strand of (L-) LK$_7\beta$ adopts a conformation that resembles an extended β-strand structure (Figure 6d). Remarkably, the isolated strand of (L-) LK$_7\beta$ adopts a β-strand-like conformation even in the total absence of stabilizing interstrand hydrogen bonds.

For all the LK$_7\beta$ variants studied here, tilt angle analyses show that the leucine side chains point toward the air and the lysine side chains point toward the water phase. This strong preference persists strongly even for the mixed chirality (L-Leu)/(D-Lys) system (Figure 7c,d). In line with previous studies,[86] our results demonstrate that peptides adapt their architectures in line with the preferences of hydrophobic and hydrophilic side chains toward the most stable phase even if these preferences incur large energetic costs by abolishing interstrand hydrogen bonds. Our results go further, though: they also show that side chain dynamics at the interface can be independent of chiral inversions along the peptide backbone.

Thus, our results suggest that interfacial (L-) and (D-) β-strand formation (and possibly β-sheet formation) can be driven from the alternating hydrophobicity and hydrophilicity of the peptide side chains, more so than the disposition of the peptide backbone to form interstrand hydrogen bonds. It is notable, however, that even this extremely strong alternating hydrophobic/hydrophilic preference can fail to form secondary structure if there is (L-)/(D-) heterochirality. Note that, due to the chiral inversion in the lysine residues, the formation of an antiparallel β-sheet secondary structure would require the positioning of both leucine and lysine side chains on the *same* side of the sheet. This arrangement of side chains not only imposes steric hindrances on the β-sheet, due to the presence of bulky neighbor groups, but also prevents the hydrophobic or hydrophilic groups to be directed toward the more stable phase, completely destabilizing the β-sheet secondary structure at the interface. Because of the ability of VSFG to probe both local chemical functionalities and macroscopic chirality, these results can guide researcher expectations about the VSFG optical responses of proteins at interfaces.

Experimental Support That Chiral VSFG Response Is Due to Macroscopic Chirality of β-Sheets. The achiral and chiral VSFG results in Figure 3a,b show that acid denaturation of (L-) LK$_7\beta$ and consequent loss of secondary structure do not silence the CH_2 FR mode at 2913 cm^{-1}. In fact, the achiral C−H stretch spectrum of (L-) LK$_7\beta$ is almost indistinguishable at pH = 7 or pH = 2 (Figure 3a). But the chiral amide I/amide II signal, which is indicative of antiparallel β-sheets in (L-) and (D-) LK$_7\beta$, is very strong at pH = 7 and almost completely abolished at pH = 2 (Figure 3b).

Intriguingly, our MD simulations of a single strand of (L-) LK$_7\beta$ (Figure 6d) offer insight about why the VSFG optical activities of the achiral C−H modes are insensitive to acid denaturation. The orientations of the C−H stretching modes are virtually unchanged when (L-) LK$_7\beta$ exists as an isolated β-strand (Figures S9 and S10) versus in antiparallel β-sheets (Figure 7a,b). On the basis of this result and our vibrational mode assignments for the C−H stretching region, one could have expected that the *achiral* C−H spectrum at denatured pH = 2 versus native pH = 7 would be relatively indistinguishable.

In contrast, our research group previously showed that (L-) LK$_7\beta$ at the air−water interface shows no *chiral* C−H response at pH = 2.[62] However, our MD simulations (Figure 6d) show that even one (L-) LK$_7\beta$ will form a β-strand due to the preference of its hydrophilic and hydrophobic side chains to have structure at the interface. Therefore, our studies lend critical support for the theory of Simpson[41,42] that suggests the chiral VSFG optical response of LK$_7\beta$ is due to *macroscopic* chirality of antiparallel β-sheets.

CONCLUSIONS

We have applied VSFG spectroscopy in combination with DFT calculations and MD simulations to investigate the effects of chiral inversions of amino acids along the full length of a model antiparallel β-sheet peptide at interfaces. We learned how chiral inversions perturb the local structure of the peptide at the interface, and how such perturbations consequently disrupt the peptide secondary structure. The combination of VSFG experiments, DFT calculations of the VSFG optical response, and MD analyses of the peptide at the air−water interface show that, regardless of amino acid chirality, the peptide side chains exhibit strong preferences for either the hydrophobic or hydrophilic phases. The peptide backbone adopts a conformation that accommodates these preferences within steric constraints. In the case of alternating (L-)/(D-) chirality in LK$_7\beta$, for instance, this results in a complete loss of the antiparallel β-sheet secondary structure. Future studies that

DOI: 10.1021/acs.jpcb.9b04029
J. Phys. Chem. B 2019, 123, 5769−5781

systematically address the effects of differently patterned (nonalternating) chiral inversions on the protein backbone, or extend these investigations to the study of protein−protein interfaces, will help to define the rules that link protein primary structure to secondary and tertiary structures. Such work should be particularly relevant for *de novo* design of unnatural protein structures with novel functions. Finally, controllable perturbations to protein molecular structure (e.g., chiral inversions, chemical and thermal denaturation, side chain modification, etc.) can be employed as critical tests of chiral VSFG theory.

■ ASSOCIATED CONTENT

Supporting Information

The Supporting Information is available free of charge on the ACS Publications website at DOI: 10.1021/acs.jpcb.9b04029.

ATR-FTIR of $LK_7\beta$ variants, anharmonic analyses of leucine and lysine residues, normal-mode analyses of $LK_3\beta$-model, per residue free energy profiles of $LK_7\beta$ variants, time evolution of side chain orientations of (L-) $LK_7\beta$, strand dynamics of (L-Leu)/(D-Lys) $LK_7\beta$, and supplementary analyses of side chain orientations (PDF)

■ AUTHOR INFORMATION

Corresponding Authors

*E-mail: elsa.yan@yale.edu.

*E-mail: victor.batista@yale.edu.

ORCID

Ethan A. Perets: 0000-0001-9554-776X

Pablo E. Videla: 0000-0003-0742-0342

Elsa C. Y. Yan: 0000-0002-3583-1627

Victor S. Batista: 0000-0002-3262-1237

Author Contributions

§E.A.P. and P.E.V. made equal contributions.

Notes

The authors declare no competing financial interest.

■ ACKNOWLEDGMENTS

E.A.P. is supported by the NIH (5T32GM008283-30). V.S.B. acknowledges support from the NIH Grant GM106121 and supercomputer time from the National Energy Research Scientific Computing Center (NERSC).

■ REFERENCES

(1) Ketchem, R. R.; Hu, W.; Cross, T. A. High-resolution conformation of gramicidin A in a lipid bilayer by solid-state NMR. *Science* **1993**, *261*, 1457.

(2) Nicholson, L. K.; Cross, T. A. Gramicidin cation channel: an experimental determination of the right-handed helix sense and verification of.beta.-type hydrogen bonding. *Biochemistry* **1989**, *28*, 9379−9385.

(3) Finking, R.; Marahiel, M. A. Biosynthesis of Nonribosomal Peptides. *Annu. Rev. Microbiol.* **2004**, *58*, 453−488.

(4) Kessler, N.; Schuhmann, H.; Morneweg, S.; Linne, U.; Marahiel, M. A. The Linear Pentadecapeptide Gramicidin Is Assembled by Four Multimodular Nonribosomal Peptide Synthetases That Comprise 16 Modules with 56 Catalytic Domains. *J. Biol. Chem.* **2004**, *279*, 7413−7419.

(5) Durani, S. Protein Design with l- and d-α-Amino Acid Structures as the Alphabet. *Acc. Chem. Res.* **2008**, *41*, 1301−1308.

(6) Huang, P.-S.; Boyken, S. E.; Baker, D. The coming of age of de novo protein design. *Nature* **2016**, *537*, 320.

(7) Lam, K. S.; Salmon, S. E.; Hersh, E. M.; Hruby, V. J.; Kazmierski, W. M.; Knapp, R. J. A new type of synthetic peptide library for identifying ligand-binding activity. *Nature* **1991**, *354*, 82.

(8) Oliva, R.; Chino, M.; Pane, K.; Pistorio, V.; De Santis, A.; Pizzo, E.; D'Errico, G.; Pavone, V.; Lombardi, A.; Del Vecchio, P.; et al. Exploring the role of unnatural amino acids in antimicrobial peptides. *Sci. Rep.* **2018**, *8*, 8888.

(9) Milton, R. C.; Milton, S. C.; Kent, S. B. Total chemical synthesis of a D-enzyme: the enantiomers of HIV-1 protease show reciprocal chiral substrate specificity [corrected]. *Science* **1992**, *256*, 1445.

(10) Mahalakshmi, R.; Balaram, P. In *D-Amino Acids: A New Frontier in Amino Acid and Protein Research*; Konno, R., Ed.; Nova Science Publisher: New York, 2007.

(11) Buri, M. V.; Domingues, T. M.; Paredes-Gamero, E. J.; Casaes-Rodrigues, R. L.; Rodrigues, E. G.; Miranda, A. Resistance to Degradation and Cellular Distribution are Important Features for the Antitumor Activity of Gomesin. *PLoS One* **2013**, *8*, e80924.

(12) Manabe, T.; Kawasaki, K. D-form KLKLLLLLKLK-NH2 peptide exerts higher antimicrobial properties than its L-form counterpart via an association with bacterial cell wall components. *Sci. Rep.* **2017**, *7*, 43384.

(13) Zerze, G. H.; Khan, M. N.; Stillinger, F. H.; Debenedetti, P. G. Computational Investigation of the Effect of Backbone Chiral Inversions on Polypeptide Structure. *J. Phys. Chem. B* **2018**, *122*, 6357−6363.

(14) Shen, Y. R. Surface properties probed by second-harmonic and sum-frequency generation. *Nature* **1989**, *337*, 519.

(15) Shen, L.; Ulrich, N. W.; Mello, C. M.; Chen, Z. Determination of conformation and orientation of immobilized peptides and proteins at buried interfaces. *Chem. Phys. Lett.* **2015**, *619*, 247−255.

(16) Wang, Z.; Morales-Acosta, M. D.; Li, S.; Liu, W.; Kanai, T.; Liu, Y.; Chen, Y.-N.; Walker, F. J.; Ahn, C. H.; Leblanc, R. M.; et al. A narrow amide I vibrational band observed by sum frequency generation spectroscopy reveals highly ordered structures of a biofilm protein at the air/water interface. *Chem. Commun.* **2016**, *52*, 2956−2959.

(17) Xiao, D.; Fu, L.; Liu, J.; Batista, V. S.; Yan, E. C. Y. Amphiphilic Adsorption of Human Islet Amyloid Polypeptide Aggregates to Lipid/Aqueous Interfaces. *J. Mol. Biol.* **2012**, *421*, 537−547.

(18) Yan, E. C. Y.; Fu, L.; Wang, Z.; Liu, W. Biological Macromolecules at Interfaces Probed by Chiral Vibrational Sum Frequency Generation Spectroscopy. *Chem. Rev.* **2014**, *114*, 8471−8498.

(19) Fu, L.; Liu, J.; Yan, E. C. Y. Chiral Sum Frequency Generation Spectroscopy for Characterizing Protein Secondary Structures at Interfaces. *J. Am. Chem. Soc.* **2011**, *133*, 8094−8097.

(20) Fu, L.; Wang, Z.; Psciuk, B. T.; Xiao, D.; Batista, V. S.; Yan, E. C. Y. Characterization of Parallel β-Sheets at Interfaces by Chiral Sum Frequency Generation Spectroscopy. *J. Phys. Chem. Lett.* **2015**, *6*, 1310−1315.

(21) Fu, L.; Wang, Z.; Yan, E. C. Y. Chiral vibrational structures of proteins at interfaces probed by sum frequency generation spectroscopy. *Int. J. Mol. Sci.* **2011**, *12*, 9404−9425.

(22) Weidner, T.; Apte, J. S.; Gamble, L. J.; Castner, D. G. Probing the Orientation and Conformation of α-Helix and β-Strand Model Peptides on Self-Assembled Monolayers Using Sum Frequency Generation and NEXAFS Spectroscopy. *Langmuir* **2010**, *26*, 3433−3440.

(23) Wang, J.; Chen, X.; Clarke, M. L.; Chen, Z. Detection of chiral sum frequency generation vibrational spectra of proteins and peptides at interfaces in situ. *Proc. Natl. Acad. Sci. U. S. A.* **2005**, *102*, 4978.

(24) Shen, Y. R. *The Principles of Nonlinear Optics*; Wiley-Interscience: New York, 1984.

(25) Boyd, R. *Nonlinear Optics*; Academic Press: Cambridge, MA, 2008.

(26) Eisenthal, K. B. Liquid Interfaces Probed by Second-Harmonic and Sum-Frequency Spectroscopy. *Chem. Rev.* **1996**, *96*, 1343−1360.

(27) Wang, H.-F.; Gan, W.; Lu, R.; Rao, Y.; Wu, B.-H. Quantitative spectral and orientational analysis in surface sum frequency generation

DOI: 10.1021/acs.jpcb.9b04029
J. Phys. Chem. B 2019, 123, 5769−5781

vibrational spectroscopy (SFG-VS). *Int. Rev. Phys. Chem.* **2005**, *24*, 191−256.
(28) Lambert, A. G.; Davies, P. B.; Neivandt, D. J. Implementing the Theory of Sum Frequency Generation Vibrational Spectroscopy: A Tutorial Review. *Appl. Spectrosc. Rev.* **2005**, *40*, 103−145.
(29) Zhuang, X.; Miranda, P. B.; Kim, D.; Shen, Y. R. Mapping molecular orientation and conformation at interfaces by surface nonlinear optics. *Phys. Rev. B: Condens. Matter Mater. Phys.* **1999**, *59*, 12632−12640.
(30) Wang, H.-F.; Velarde, L.; Gan, W.; Fu, L. Quantitative Sum-Frequency Generation Vibrational Spectroscopy of Molecular Surfaces and Interfaces: Lineshape, Polarization, and Orientation. *Annu. Rev. Phys. Chem.* **2015**, *66*, 189−216.
(31) Chen, X.; Sagle, L. B.; Cremer, P. S. Urea Orientation at Protein Surfaces. *J. Am. Chem. Soc.* **2007**, *129*, 15104−15105.
(32) Schmüser, L.; Roeters, S.; Lutz, H.; Woutersen, S.; Bonn, M.; Weidner, T. Determination of Absolute Orientation of Protein α-Helices at Interfaces Using Phase-Resolved Sum Frequency Generation Spectroscopy. *J. Phys. Chem. Lett.* **2017**, *8*, 3101−3105.
(33) Ji, N.; Shen, Y.-R. Sum frequency vibrational spectroscopy of leucine molecules adsorbed at air−water interface. *J. Chem. Phys.* **2004**, *120*, 7107−7112.
(34) Ma, G.; Allen, H. C. DPPC Langmuir Monolayer at the Air−Water Interface: Probing the Tail and Head Groups by Vibrational Sum Frequency Generation Spectroscopy. *Langmuir* **2006**, *22*, 5341−5349.
(35) Guyot-Sionnest, P.; Hunt, J. H.; Shen, Y. R. Sum-frequency vibrational spectroscopy of a Langmuir film: Study of molecular orientation of a two-dimensional system. *Phys. Rev. Lett.* **1987**, *59*, 1597−1600.
(36) Himmelhaus, M.; Eisert, F.; Buck, M.; Grunze, M. Self-Assembly of n-Alkanethiol Monolayers. A Study by IR−Visible Sum Frequency Spectroscopy (SFG). *J. Phys. Chem. B* **2000**, *104*, 576−584.
(37) Lu, R.; Gan, W.; Wu, B.-h.; Chen, H.; Wang, H.-f. Vibrational Polarization Spectroscopy of CH Stretching Modes of the Methylene Group at the Vapor/Liquid Interfaces with Sum Frequency Generation. *J. Phys. Chem. B* **2004**, *108*, 7297−7306.
(38) Lu, R.; Gan, W.; Wu, B.-h.; Zhang, Z.; Guo, Y.; Wang, H.-f. C−H Stretching Vibrations of Methyl, Methylene and Methine Groups at the Vapor/Alcohol (n = 1−8) Interfaces. *J. Phys. Chem. B* **2005**, *109*, 14118−14129.
(39) Fu, L.; Zhang, Y.; Wei, Z.-H.; Wang, H.-F. Intrinsic Chirality and Prochirality at Air/R-(+)- and S-(−)-Limonene Interfaces: Spectral Signatures With Interference Chiral Sum-Frequency Generation Vibrational Spectroscopy. *Chirality* **2014**, *26*, 509−520.
(40) Wang, H.-F. In *Comprehensive Chiroptical Spectroscopy*; Berova, N., Polavarapu, P. L., Nakanishi, K., Woody, R. W., Eds.; John Wiley & Sons, Inc.: Hoboken, 2011.
(41) Moad, A. J.; Simpson, G. J. A Unified Treatment of Selection Rules and Symmetry Relations for Sum-Frequency and Second Harmonic Spectroscopies. *J. Phys. Chem. B* **2004**, *108*, 3548−3562.
(42) Simpson, G. J. Molecular Origins of the Remarkable Chiral Sensitivity of Second-Order Nonlinear Optics. *ChemPhysChem* **2004**, *5*, 1301−1310.
(43) Ma, G.; Liu, J.; Fu, L.; Yan, E. C. Y. Probing Water and Biomolecules at the Air—Water Interface with a Broad Bandwidth Vibrational Sum Frequency Generation Spectrometer from 3800 to 900 cm−1. *Appl. Spectrosc.* **2009**, *63*, 528−537.
(44) Best, R. B.; Zhu, X.; Shim, J.; Lopes, P. E. M.; Mittal, J.; Feig, M.; MacKerell, A. D. Optimization of the Additive CHARMM All-Atom Protein Force Field Targeting Improved Sampling of the Backbone ϕ, ψ and Side-Chain χ1 and χ2 Dihedral Angles. *J. Chem. Theory Comput.* **2012**, *8*, 3257−3273.
(45) Jorgensen, W. L.; Chandrasekhar, J.; Madura, J. D.; Impey, R. W.; Klein, M. L. Comparison of simple potential functions for simulating liquid water. *J. Chem. Phys.* **1983**, *79*, 926−935.
(46) Phillips, J. C.; Braun, R.; Wang, W.; Gumbart, J.; Tajkhorshid, E.; Villa, E.; Chipot, C.; Skeel, R. D.; Kalé, L.; Schulten, K. Scalable molecular dynamics with NAMD. *J. Comput. Chem.* **2005**, *26*, 1781−1802.
(47) Miyamoto, S.; Kollman, P. A. Settle: An analytical version of the SHAKE and RATTLE algorithm for rigid water models. *J. Comput. Chem.* **1992**, *13*, 952−962.
(48) Humphrey, W.; Dalke, A.; Schulten, K. VMD: Visual molecular dynamics. *J. Mol. Graphics* **1996**, *14*, 33−38.
(49) Frisch, M. J.; Trucks, G. W.; Schlegel, H. B.; Scuseria, G. E.; Robb, M. A.; Cheeseman, J. R.; Scalmani, G.; Barone, V.; Petersson, G. A.; Nakatsuji, H.; et al. *Gaussian 09 Rev. E.01*; Gaussian: Wallingford, CT, 2009.
(50) Becke, A. D. Density-functional thermochemistry. III. The role of exact exchange. *J. Chem. Phys.* **1993**, *98*, 5648−5652.
(51) Hariharan, P. C.; Pople, J. A. The influence of polarization functions on molecular orbital hydrogenation energies. *Theor. Chim. Acta* **1973**, *28*, 213−222.
(52) Anfuso, C. L.; Snoeberger, R. C.; Ricks, A. M.; Liu, W.; Xiao, D.; Batista, V. S.; Lian, T. Covalent Attachment of a Rhenium Bipyridyl CO2 Reduction Catalyst to Rutile TiO2. *J. Am. Chem. Soc.* **2011**, *133*, 6922−6925.
(53) Anfuso, C. L.; Xiao, D.; Ricks, A. M.; Negre, C. F. A.; Batista, V. S.; Lian, T. Orientation of a Series of CO2 Reduction Catalysts on Single Crystal TiO2 Probed by Phase-Sensitive Vibrational Sum Frequency Generation Spectroscopy (PS-VSFG). *J. Phys. Chem. C* **2012**, *116*, 24107−24114.
(54) Fu, L.; Xiao, D.; Wang, Z.; Batista, V. S.; Yan, E. C. Y. Chiral Sum Frequency Generation for In Situ Probing Proton Exchange in Antiparallel β-Sheets at Interfaces. *J. Am. Chem. Soc.* **2013**, *135*, 3592−3598.
(55) Clark, M. L.; Rudshteyn, B.; Ge, A.; Chabolla, S. A.; Machan, C. W.; Psciuk, B. T.; Song, J.; Canzi, G.; Lian, T.; Batista, V. S.; et al. Orientation of Cyano-Substituted Bipyridine Re(I) fac-Tricarbonyl Electrocatalysts Bound to Conducting Au Surfaces. *J. Phys. Chem. C* **2016**, *120*, 1657−1665.
(56) Ge, A.; Rudshteyn, B.; Psciuk, B. T.; Xiao, D.; Song, J.; Anfuso, C. L.; Ricks, A. M.; Batista, V. S.; Lian, T. Surface-Induced Anisotropic Binding of a Rhenium CO2-Reduction Catalyst on Rutile TiO2(110) Surfaces. *J. Phys. Chem. C* **2016**, *120*, 20970−20977.
(57) Ge, A.; Videla, P. E.; Lee, G. L.; Rudshteyn, B.; Song, J.; Kubiak, C. P.; Batista, V. S.; Lian, T. Interfacial Structure and Electric Field Probed by in Situ Electrochemical Vibrational Stark Effect Spectroscopy and Computational Modeling. *J. Phys. Chem. C* **2017**, *121*, 18674−18682.
(58) Ge, A.; Videla, P. E.; Rudshteyn, B.; Liu, Q.; Batista, V. S.; Lian, T. Dopant-Dependent SFG Response of Rhenium CO2 Reduction Catalysts Chemisorbed on SrTiO3 (100) Single Crystals. *J. Phys. Chem. C* **2018**, *122*, 13944−13952.
(59) DeGrado, W. F.; Lear, J. D. Induction of peptide conformation at apolar water interfaces. 1. A study with model peptides of defined hydrophobic periodicity. *J. Am. Chem. Soc.* **1985**, *107*, 7684−7689.
(60) Phillips, D. C.; York, R. L.; Mermut, O.; McCrea, K. R.; Ward, R. S.; Somorjai, G. A. Side Chain, Chain Length, and Sequence Effects on Amphiphilic Peptide Adsorption at Hydrophobic and Hydrophilic Surfaces Studied by Sum-Frequency Generation Vibrational Spectroscopy and Quartz Crystal Microbalance. *J. Phys. Chem. C* **2007**, *111*, 255−261.
(61) Stokes, G. Y.; Gibbs-Davis, J. M.; Boman, F. C.; Stepp, B. R.; Condie, A. G.; Nguyen, S. T.; Geiger, F. M. Making "Sense" of DNA. *J. Am. Chem. Soc.* **2007**, *129*, 7492−7493.
(62) Wang, Z.; Fu, L.; Yan, E. C. Y. C−H Stretch for Probing Kinetics of Self-Assembly into Macromolecular Chiral Structures at Interfaces by Chiral Sum Frequency Generation Spectroscopy. *Langmuir* **2013**, *29*, 4077−4083.
(63) Bloino, J.; Barone, V. A second-order perturbation theory route to vibrational averages and transition properties of molecules: General formulation and application to infrared and vibrational circular dichroism spectroscopies. *J. Chem. Phys.* **2012**, *136*, 124108.

DOI: 10.1021/acs.jpcb.9b04029
J. Phys. Chem. B 2019, 123, 5769−5781

(64) Yagi, K.; Hirata, S.; Hirao, K. Vibrational quasi-degenerate perturbation theory: applications to fermi resonance in CO2, H2CO, and C6H6. *Phys. Chem. Chem. Phys.* **2008**, *10*, 1781−1788.
(65) Barone, V.; Bloino, J.; Guido, C. A.; Lipparini, F. A fully automated implementation of VPT2 Infrared intensities. *Chem. Phys. Lett.* **2010**, *496*, 157−161.
(66) Biczysko, M.; Bloino, J.; Carnimeo, I.; Panek, P.; Barone, V. Fully ab initio IR spectra for complex molecular systems from perturbative vibrational approaches: Glycine as a test case. *J. Mol. Struct.* **2012**, *1009*, 74−82.
(67) Bowman, J. M.; Carrington, T.; Meyer, H.-D. Variational quantum approaches for computing vibrational energies of polyatomic molecules. *Mol. Phys.* **2008**, *106*, 2145−2182.
(68) Roy, T. K.; Gerber, R. B. Vibrational self-consistent field calculations for spectroscopy of biological molecules: new algorithmic developments and applications. *Phys. Chem. Chem. Phys.* **2013**, *15*, 9468−9492.
(69) Qu, C.; Bowman, J. M. Quantum approaches to vibrational dynamics and spectroscopy: is ease of interpretation sacrificed as rigor increases? *Phys. Chem. Chem. Phys.* **2019**, *21*, 3397.
(70) Ho, J.; Psciuk, B. T.; Chase, H. M.; Rudshteyn, B.; Upshur, M. A.; Fu, L.; Thomson, R. J.; Wang, H.-F.; Geiger, F. M.; Batista, V. S. Sum Frequency Generation Spectroscopy and Molecular Dynamics Simulations Reveal a Rotationally Fluid Adsorption State of α-Pinene on Silica. *J. Phys. Chem. C* **2016**, *120*, 12578−12589.
(71) Jetzki, M.; Luckhaus, D.; Signorell, R. Fermi resonance and conformation in glycolaldehyde particles. *Can. J. Chem.* **2004**, *82*, 915−924.
(72) Guo, Z.; Zheng, W.; Hamoudi, H.; Dablemont, C.; Esaulov, V. A.; Bourguignon, B. On the chain length dependence of CH3 vibrational mode relative intensities in sum frequency generation spectra of self assembled alkanethiols. *Surf. Sci.* **2008**, *602*, 3551−3559.
(73) York, R. L.; Browne, W. K.; Geissler, P. L.; Somorjai, G. A. Peptides Adsorbed on Hydrophobic Surfaces—A Sum Frequency Generation Vibrational Spectroscopy and Modeling Study. *Isr. J. Chem.* **2007**, *47*, 51−58.
(74) Watry, M. R.; Richmond, G. L. Orientation and Conformation of Amino Acids in Monolayers Adsorbed at an Oil/Water Interface As Determined by Vibrational Sum-Frequency Spectroscopy. *J. Phys. Chem. B* **2002**, *106*, 12517−12523.
(75) Holinga, G. J.; York, R. L.; Onorato, R. M.; Thompson, C. M.; Webb, N. E.; Yoon, A. P.; Somorjai, G. A. An SFG Study of Interfacial Amino Acids at the Hydrophilic SiO2 and Hydrophobic Deuterated Polystyrene Surfaces. *J. Am. Chem. Soc.* **2011**, *133*, 6243−6253.
(76) York, R. L.; Mermut, O.; Phillips, D. C.; McCrea, K. R.; Ward, R. S.; Somorjai, G. A. Influence of Ionic Strength on the Adsorption of a Model Peptide on Hydrophilic Silica and Hydrophobic Polystyrene Surfaces: Insight from SFG Vibrational Spectroscopy. *J. Phys. Chem. C* **2007**, *111*, 8866−8871.
(77) Mermut, O.; Phillips, D. C.; York, R. L.; McCrea, K. R.; Ward, R. S.; Somorjai, G. A. In Situ Adsorption Studies of a 14-Amino Acid Leucine-Lysine Peptide onto Hydrophobic Polystyrene and Hydrophilic Silica Surfaces Using Quartz Crystal Microbalance, Atomic Force Microscopy, and Sum Frequency Generation Vibrational Spectroscopy. *J. Am. Chem. Soc.* **2006**, *128*, 3598−3607.
(78) Towse, C.-L.; Hopping, G.; Vulovic, I.; Daggett, V. Nature versus design: the conformational propensities of d-amino acids and the importance of side chain chirality. *Protein Eng., Des. Sel.* **2014**, *27*, 447−455.
(79) Fairman, R.; Anthony-Cahill, S. J.; DeGrado, W. F. The helix-forming propensity of D-alanine in a right-handed.alpha.-helix. *J. Am. Chem. Soc.* **1992**, *114*, 5458−5459.
(80) Hermans, J.; Anderson, A. G.; Yun, R. H. Differential helix propensity of small apolar side chains studied by molecular dynamics simulations. *Biochemistry* **1992**, *31*, 5646−5653.
(81) Krause, E.; Beyermann, M.; Dathe, M.; Rothemund, S.; Bienert, M. Location of an Amphipathic.alpha.-Helix in Peptides Using Reversed-Phase HPLC Retention Behavior of D-Amino Acid Analogs. *Anal. Chem.* **1995**, *67*, 252−258.
(82) Krause, E.; Bienert, M.; Schmieder, P.; Wenschuh, H. The Helix-Destabilizing Propensity Scale of d-Amino Acids: The Influence of Side Chain Steric Effects. *J. Am. Chem. Soc.* **2000**, *122*, 4865−4870.
(83) Nanda, V.; DeGrado, W. F. Simulated Evolution of Emergent Chiral Structures in Polyalanine. *J. Am. Chem. Soc.* **2004**, *126*, 14459−14467.
(84) Weidner, T.; Breen, N. F.; Li, K.; Drobny, G. P.; Castner, D. G. Sum frequency generation and solid-state NMR study of the structure, orientation, and dynamics of polystyrene-adsorbed peptides. *Proc. Natl. Acad. Sci. U. S. A.* **2010**, *107*, 13288.
(85) Donovan, M. A.; Yimer, Y. Y.; Pfaendtner, J.; Backus, E. H. G.; Bonn, M.; Weidner, T. Ultrafast Reorientational Dynamics of Leucine at the Air−Water Interface. *J. Am. Chem. Soc.* **2016**, *138*, 5226−5229.
(86) Donovan, M. A.; Lutz, H.; Yimer, Y. Y.; Pfaendtner, J.; Bonn, M.; Weidner, T. LK peptide side chain dynamics at interfaces are independent of secondary structure. *Phys. Chem. Chem. Phys.* **2017**, *19*, 28507−28511.

DOI: 10.1021/acs.jpcb.9b04029
J. Phys. Chem. B 2019, 123, 5769−5781